Excitonic approach to the ultrafast optical response of semiconductors

Dawei Wang,[1] Margaret Hawton,[2] and Marc M. Dignam[1]

[1]*Department of Physics, Queen's University, Kingston, Ontario, Canada K7L 3N6*
[2]*Department of Physics, Lakehead University, Thunder Bay, Ontario, Canada P7B 5E1*
(Received 26 June 2007; published 12 September 2007)

We present a theoretical approach to treating the coherent dynamics of optically generated charge carriers in semiconductors using an excitonic basis. In contrast to the semiconductor Bloch equations, our approach treats intraband correlations without factorization. It also includes phase space filling effects that have generally been omitted in previous excitonic treatments of coherent dynamics. We show that, in the coherent limit, where the intraband dephasing time and population decay time are both equal to half of the interband dephasing time, our excitonic approach agrees with the semiconductor Bloch equations to at least third order in the optical field, but that it differs significantly in more general situations. Our excitonic equations are shown to be particularly applicable in systems, such as biased semiconductor superlattices, where bound excitons dominate the optical response and where intraband correlations play a central role. Using a simple model of a nanoring, we show how the spectral shifts in the interband response can be explained in terms of phase-space-filling-induced excitonic population dynamics.

I. INTRODUCTION

The ultrafast spectroscopy of semiconductor nanostructures provides great insight into the underlying physical dynamical processes in these systems. Radiation emitted by the photoexcited charge carriers in nonequilibrium states discloses fundamental information about single-particle dynamics as well as many-body correlations. Many different experimental techniques have been developed to investigate different aspects of these dynamical processes in semiconductors.[1,2] Time-resolved photoluminescence and pump-probe spectroscopy are often used to study carrier relaxation processes, while four-wave-mixing spectroscopy can provide direct information on the dynamics and decay of the interband polarization. Degenerate four-wave-mixing (DFWM) techniques and terahertz emission spectroscopy have also been used to probe intraband processes in asymmetric structures such as coupled double quantum wells[2] and biased semiconductor superlattices (BSSLs).[3,4] In all of these systems, many-body effects can influence carrier dynamics profoundly at moderate to high carrier densities. Such effects include biexcitons,[5,6] screening,[1] excitation-induced dephasing,[7] self-induced intraband fields,[8] and phase space filling (PSF).[9] Thus, in the theoretical treatment of these systems, it is important that the theoretical formalism employed is able to capture the key many-body effects particular to the system being investigated while remaining computationally tractable.

Many theoretical approaches have been developed and refined for the treatment of ultrafast phenomena in semiconductors. Nonequilibrium Green's function and density matrix techniques are amongst the most commonly used methods.[1] The well-known semiconductor Bloch equations (SBEs) are based on the second approach,[10] as are the dynamics controlled truncation (DCT) equations.[11]

The density matrix approach yields an infinite hierarchy of operator equations, which is the quantum counterpart of the Bogoliubov-Born-Green-Kirkwood-Yvon hierarchy in classical gas dynamics.[1] The expectation value of the operators can be used to calculate various physical quantities, such as charge-carrier (electron, hole) distributions, current density, or electronic polarizations. To obtain a group of closed equations, some approximations are required. One approach is to truncate the equations to a certain order in the optical field.[11,12] This has the advantage that the results are exact to a specified order in the optical field. However, at high laser intensities, such a perturbative approach can break down.[8,13–15] An alternative approach is to factorize the expectation value of several operators into a product of expectation values with fewer operators.[10] The factorization approach is called a correlation expansion; it effectively neglects correlation functions involving more than a given number of particles. Depending on the number of operators retained in the remaining correlation functions, the resulting equations can be used to describe various dynamical processes in semiconductors, such as single-particle dynamics, carrier-phonon interactions, dynamic screening, and carrier-carrier interactions.[1,12]

One of the most successful approaches to treating ultrafast phenomena are the SBEs. They are well accepted and have been successfully used to treat a large number of coherent effects in semiconductors including the dynamic Stark effect and Rabi oscillations, and to model various pump-probe and four-wave-mixing experiments.[2,10] They have the advantage that they are nonperturbative in the optical field and are relatively simple and computationally efficient. However, they have two drawbacks that make them inappropriate for use in certain systems. First, they omit higher-order correlations beyond the random phase approximation (RPA) or Hartree-Fock approximation. Second, because they effectively factorize an intraband correlation function into the product of two interband correlation functions (see Sec. III B), they incorrectly treat intraband correlations[16] except in the so-called *coherent limit*[16] where $T_{\text{decay}}=T_{\text{intra}}=T_{\text{inter}}/2$, i.e., when the population decay time and the intraband dephasing time are both equal to half of the interband dephasing time. Thus, in general they are inappropriate for use in systems where in-

traband correlations are important. Both of these difficulties with the SBEs can be addressed by employing either a higher-order cluster expansion approach or a higher-order DCT approach. However, such approaches are computationally very taxing and are generally prohibitive for use in complicated systems such as BSSLs. The aim of this paper is to introduce a formalism to treat ultrafast dynamics in semiconductor systems in which excitonic effects and intraband dynamics play a dominant role but correlations beyond the RPA are not essential.

One class of systems in which excitons dominate the response and in which intraband coherences play a central role are asymmetric or biased coupled quantum wells and superlattices. Consider, for example, a BSSL. If an undoped BSSL is excited by a short optical pulse with a central energy that is below the energy of $1s$ excitons in the $n=0$ excitonic Wannier-Stark-Ladder (WSL) level, a large intraband response that is dominated by the dynamics of $1s$ excitons is generated.[15] The coherent excitonic wave packets that are created oscillate in space at the Bloch-oscillation frequency. These oscillations result from intraband coherences between different excitonic WSL levels. The resulting self-induced intraband electric fields can give rise to such effects as the transformation of Bloch oscillations into plasma oscillations[8] and oscillations in spectral peak positions in DFWM experiments.[4,13] We have shown that at moderate densities, the optical and terahertz response in BSSLs is well described using an *excitonic formalism* with exciton-exciton interactions included in a mean-field approximation via the intraband polarization.[8] Although successful, these excitonic treatments did not include PSF or exchange. Before discussing the PSF problem, we first examine the potential advantages of excitonic approaches to carrier dynamics.

In comparison to approaches that employ an electron-hole basis, approaches that use an *excitonic basis* have several advantages. First, since excitonic states are the lowest-energy excited states, they often dominate the optical response. Using an excitonic basis thus allows us to relate absorption or photoluminescence spectra directly to exciton dynamics. Second, an excitonic basis naturally includes the important intraexcitonic electron-hole correlations; since excitons are neutral particles, the remaining exciton-exciton correlations are generally weak in the low to moderate exciton density regime and can often be treated approximately in a mean-field way. Third, because dephasing effects are often included approximately or phenomenologically, the separation of dephasing times from population decay times is more accurate if the populations considered are excitons (the two-particle eigenstates of the system) than if they are electrons and holes.[8,13–15] Finally, perhaps the most important advantage of using an excitonic basis is that the intraband correlation functions can be retained in an unfactorized form without requiring the use of a prohibitive number of dynamical equations. The resulting increase in computational efficiency makes it possible to model complicated systems, such as BSSLs, that exhibit strong effects from intraband correlations.

Previously, most excitonic approaches to treating ultrafast dynamics in complicated systems have neglected the PSF effects associated with the nonbosonic nature of excitons.

Composed of an electron-hole pair, a bound exciton can be treated effectively as a boson at low carrier densities. However, as the density increases, the composite nature of excitons becomes increasingly important, leading to the so-called PSF that arises from the Fermi statistics of electrons and holes. In a free electron-hole basis, this effect can be included naturally through the Fermi statistics. Using an excitonic basis, there is no obvious simple way to treat PSF effects or to know at what precise density PSF will become important. Various methods, such as bosonization[17] and commutation techniques,[18,19] have been proposed to treat this problem, but there is still considerable controversy in the field[20–22] and there is no clear consensus as to the best way to address this problem.

In this paper, we develop a set of excitonic equations (EXEs) to model the nonlinear response of semiconductor systems to ultrashort optical pulses. These equations treat intraband polarization without factorization and include PSF and exchange effects. These EXEs offer an approach to the ultrafast response of bulk and nanostructured semiconductors that exploits the simplicity of an excitonic basis, without having to discard the important effects of phase space filling. To demonstrate the properties and advantages of our approach, we apply our formalism to a simple model of a nanoring, and compare the interband polarization calculated using our EXEs to those obtained using the SBEs. We demonstrate that our approach agrees with the SBEs in the coherent limit to at least third order in the optical field, but that it can yield significantly different results for general interband dephasing, intraband dephasing, and population decay times. These results confirm the validity of our approach and point to their importance in treating systems with strong intraband correlations.

This paper is organized as follows. In Sec. II, the Usui transformation is applied to obtain the commutation relations for the quasiboson pair space creation and annihilation operators that are used to derive quasiboson dynamic equations. In Sec. III we discuss the factorization employed to obtain a closed set of quasiboson dynamic equations and derive both the SBEs and the EXEs from these equations. In Sec. IV, we apply both the SBEs and EXEs to a model system to demonstrate the differences between the two approaches and we discuss their suitability for modeling different systems. Finally, in Sec. V, we present our conclusions.

II. QUASIBOSON DYNAMIC EQUATIONS

In this section, we derive the Hamiltonian as well as the dynamic equations for electron-hole pairs in the quasiboson (qboson) pair space. These equations are used in the next section to derive both the SBEs and our EXEs.

A. Usui transformation and the quasiboson commutation relations

In this section, we use the Usui transformation to transform from a basis of electrons and holes into a qboson pair basis. This transformation yields the commutation relations and the Hamiltonian in the qboson pair space.

The Usui transformation[23] connects the free electron and hole fermion space to the qboson pair space with the operator

$$U = P_F \exp\left(\sum_{k_e, k_h} \widetilde{B}^\dagger_{k_e, k_h} \beta_{k_h} \alpha_{k_e} \right) P_B, \qquad (1)$$

where P_F and P_B are projection operators onto the fermion space and qboson pair space vacuums, $|0\rangle_F$ and $|0\rangle_B$, respectively; $\widetilde{B}^\dagger_{k_e, k_h}$ is the creation operator for an electron-hole pair in qboson pair space, while α_{k_e} and β_{k_h} are electron and hole annihilation operators in fermion space. Here k_e and k_h are the momenta of the electron and hole, respectively. The Usui transformation is not unitary in that it maps a state with many electrons and holes into a superposition state of all possible electron-hole pairings. An ordering operator O is needed to obtain a one-to-one correspondence between the fermion states and a certain subspace of the pair space. A fermion operator A_F can thus be transformed to a pair-space operator A_B using

$$A_B = O U A_F U^\dagger O^\dagger. \qquad (2)$$

The operator O is a projection operator satisfying $O^2 = O$, giving $U^\dagger O U = 1$, such that OU is unitary.

For the situations with which we are concerned, excitons have very small center-of-mass (c.m.) momenta, as they are created by photons. Since we are considering ultrafast processes, if we neglect any scattering that creates excitons with large c.m. momentum, we can take the total momentum of every exciton to be zero. For this reason, in the following the c.m. momenta are implicitly taken to be zero and are not explicitly indicated in the subscripts of the exciton creation or annihilation operators. Thus, our ordering operator O pairs electrons and holes such that $k_h = -k_e$ and we simplify our notation for the qboson pair operator to $B^\dagger_k \equiv \widetilde{B}^\dagger_{k,-k}$. Using the Usui transformation, this operator is given by

$$B^\dagger_k = O U (\alpha^\dagger_k \beta^\dagger_{-k}) U^\dagger O^\dagger. \qquad (3)$$

The commutator of B_k and $B^\dagger_{k'}$, which will be needed later in deriving dynamic equations for $B^\dagger_k$, is given by

$$[B_k, B^\dagger_{k'}] = O U [\beta_k \alpha_k, \alpha^\dagger_{k'} \beta^\dagger_{k'}] U^\dagger O^\dagger$$
$$= \delta_{k,k'} O U (1 - \alpha^\dagger_k \alpha_k - \beta^\dagger_{-k} \beta_{-k}) U^\dagger O^\dagger. \qquad (4)$$

In the above equation, $\alpha^\dagger_k \alpha_k$ ($\beta^\dagger_{-k} \beta_{-k}$) is the electron (hole) number operator for the electron (hole) state with momentum k. To obtain a closed relation, the expressions for $\alpha^\dagger_k \alpha_k$ and $\beta^\dagger_{-k} \beta_{-k}$ in pair space are needed. Using the Usui transformation, it can be shown that

$$B^\dagger_k B_k = O U (\alpha^\dagger_k \alpha_k) U^\dagger O^\dagger = O U (\beta^\dagger_{-k} \beta_{-k}) U^\dagger O^\dagger, \qquad (5)$$

which has the clear physical meaning that the number of electrons or holes equals the number of qboson electron-hole pairs in a photoexcited undoped semiconductor system. We note that Eq. (5) is only valid for electron-hole pairs with zero c.m. momentum. Thus, we obtain from Eqs. (4) and (5) the commutation relation,

$$[B_k, B^\dagger_{k'}] = \delta_{k,k'} (1 - 2 B^\dagger_k B_k). \qquad (6)$$

It is also easily shown that

$$[B^\dagger_k, B^\dagger_{k'}] = 0. \qquad (7)$$

In addition to the above commutation relations, a further condition is required to prohibit the creation of two pairs in the same state. This condition can be derived in the fermion space, and is

$$B^\dagger_k B^\dagger_k = 0. \qquad (8)$$

Because it is deceptively simple and natural, the above relation is easily overlooked. However, as shown in later sections, energy and total exciton number in the system will not be conserved after the laser pulse has passed unless this relation is properly treated in obtaining the dynamic equations for excitons.

The consistency of the three relations of Eqs. (6)–(8) can be checked by comparing the matrix elements of the pair number operator $B^\dagger_k B_k$ between states $B^\dagger_{k_1} B^\dagger_{k_2} \cdots B^\dagger_{k_N} |0\rangle$ with N electron-hole pairs (where N is an arbitrary positive integer) obtained in the two different spaces. We have calculated this in the qboson pair space using $B^\dagger_k B_k$ and the commutation relations of Eqs. (6) and (7) and in the fermion space for the states $\alpha^\dagger_{k_1} \beta^\dagger_{k_1} \alpha^\dagger_{k_2} \beta^\dagger_{k_2} \cdots \alpha^\dagger_{k_N} \beta^\dagger_{k_N} |0\rangle$ using the commutation relations for fermions. We find that these two methods indeed give identical results.

The consistency of the commutation relations can be further confirmed by calculating the commutator of $B^\dagger_p$ and $B^\dagger_k B_k$,

$$[B^\dagger_p, B^\dagger_k B_k] = -B^\dagger_k \delta_{p,k} (1 - B^\dagger_k B_k) = -\delta_{p,k} B^\dagger_k, \qquad (9)$$

which agrees with the result obtained in an electron-hole basis,

$$[\alpha^\dagger_p \beta^\dagger_{-p}, \alpha^\dagger_k \alpha_k] = -\delta_{p,k} \alpha^\dagger_k \beta^\dagger_{-k}. \qquad (10)$$

B. Hamiltonian and dynamic equations in quasiboson pair space

Using the Usui transformation, we can transform the widely used Hamiltonian H_F for a photoexcited semiconductor system in fermion space[10,24] to obtain the Hamiltonian H in the qboson pair space,[24]

$$H = H_X + H_C + H_I. \qquad (11)$$

In Eq. (11),

$$H_X = \sum_k E^0_k B^\dagger_k B_k - \sum_{k_1, k_2} V_{k_1 - k_2} B^\dagger_{k_2} B_{k_1} \qquad (12)$$

is the Hamiltonian for noninteracting qboson pairs,

$$H_C = -\sum_{k_1, k_2} V_{k_1 - k_2} B^\dagger_{k_1} B^\dagger_{k_2} B_{k_2} B_{k_1} \qquad (13)$$

describes the exchange interaction and

$$H_I = -\sum_k \boldsymbol{\mathcal{E}}(t) \cdot (\boldsymbol{M}_{cv} B_k^\dagger + \boldsymbol{M}_{cv}^* B_k) \tag{14}$$

describes the interaction of qboson pairs with the laser electric field, $\boldsymbol{\mathcal{E}}(t)$. In Eq. (12), $E_k^0 \equiv E_g + \epsilon_k^e + \epsilon_{-k}^h$, where E_g is the energy gap between the valence and the conduction band and ϵ_k^e (ϵ_{-k}^h) is the energy of a noninteracting electron (hole) with momentum $\boldsymbol{k}$ ($-\boldsymbol{k}$). In Eq. (13), V_k is the Coulomb interaction between electrons and holes. In Eq. (14), $\boldsymbol{M}_{cv} = \langle c|e\boldsymbol{r}|v\rangle$ is the interband dipole matrix element between conduction and valence band states at $\boldsymbol{k}=0$.

We use the Heisenberg equation of motion, the qboson Hamiltonian of Eq. (11), and the commutation relations of Eqs. (6) and (7) to obtain the first dynamic equation

$$
\begin{aligned}
i\hbar \frac{d}{dt} B_p^\dagger = &-\sum_k \left[(E_g + V_0 + \epsilon_p^e + \epsilon_{-p}^h)\delta_{k,p} - V_{p-k} \right] B_k^\dagger \\
&+ 2\sum_k V_{p-k} B_p^\dagger B_k^\dagger B_k - 2\sum_k V_{p-k} B_k^\dagger B_p^\dagger B_p + \boldsymbol{\mathcal{E}}(t) \cdot \boldsymbol{M}_{cv} \\
&- 2\boldsymbol{\mathcal{E}}(t) \cdot \boldsymbol{M}_{cv} B_p^\dagger B_p.
\end{aligned}
\tag{15}
$$

In this expression the first term is from the energy of a single electron-hole pair and the two terms in the second line describe exchange and PSF effects, respectively. The two terms in the last line describe the interaction of the laser field with the system; the first term is related to the linear absorption, while the second term is a PSF term that is responsible for spectral *hole burning*.

The second dynamic equation is given by

$$
\begin{aligned}
i\hbar \frac{d}{dt} (B_p^\dagger B_q) = &-\sum_k \left[(E_g + V_0 + \epsilon_p^e + \epsilon_{-p}^h)\delta_{k,p} - V_{p-k} \right] B_k^\dagger B_q \\
&+ \sum_k \left[(E_g + V_0 + \epsilon_q^e + \epsilon_{-q}^h)\delta_{k,q} - V_{q-k} \right] B_p^\dagger B_k \\
&+ 2\sum_k V_{p-k} B_p^\dagger B_k^\dagger B_k B_q - 2\sum_k V_{q-k} B_p^\dagger B_k^\dagger B_k B_q \\
&- 2\sum_k V_{p-k} B_k^\dagger B_p^\dagger B_p B_q + 2\sum_k V_{q-k} B_p^\dagger B_q^\dagger B_q B_k \\
&+ \boldsymbol{\mathcal{E}}(t) \cdot \boldsymbol{M}_{cv} B_q - \boldsymbol{\mathcal{E}}(t) \cdot \boldsymbol{M}_{cv}^* B_p^\dagger \\
&- 2\boldsymbol{\mathcal{E}}(t) \cdot \boldsymbol{M}_{cv} B_p^\dagger B_p B_q + 2\boldsymbol{\mathcal{E}}(t) \cdot \boldsymbol{M}_{cv}^* B_p^\dagger B_q^\dagger B_q.
\end{aligned}
\tag{16}
$$

On the right side of Eq. (16), the terms in the third and the fourth lines are due to the exchange interaction and PSF effects, respectively; the terms in the fifth line are related to linear absorption, while terms in the last line are the hole-burning terms.

We emphasize that the supplementary condition of Eq. (8) is essential for correct interpretation and application of the above two equations.

III. OBTAINING A GROUP OF CLOSED EQUATIONS

The dynamic equations for the statistical averages of the qboson operators can be obtained by taking the expectation

value of operators on both sides of Eqs. (15) and (16), so as to produce the correlation functions $\langle B_p^\dagger \rangle$ and $\langle B_p^\dagger B_q \rangle$ needed to calculate the interband and intraband polarizations and exciton population distribution of the system. Factorization of higher-order density matrices is then needed to obtain a closed set of dynamic equations. We factorize density matrices of three or four operators into matrices with one or two operators. This factorization is explained in Sec. III A and it provides us with the pair-space qboson dynamic equations that are shown in Eqs. (20) and (21). However, there is a key difficulty in applying these two equations directly to investigate ultrafast dynamics in semiconductors numerically: the large number of equations makes it computationally intractable for complicated systems such as BSSLs. In Secs. III B and III C, we present two different approaches to address this difficulty. The first approach employs an additional factorization that transforms these equations into the standard SBEs.[10] The second approach employs a true excitonic basis and thus enables us to reduce the basis size. This second approach is the key result of this paper; it is not only numerically tractable but also allows us to retain interband correlations that can be important in many systems.

A. Factorization of the qboson dynamic equations

Taking the expectation values of Eqs. (15) and (16) yields an infinite hierarchy of operator equations. It is well known that there are different ways to form a closed set of dynamic equations from the infinite hierarchy, e.g., perturbation in the optical field, dynamics controlled truncation, cluster expansion, etc. Much work has been done on cluster expansions that makes it possible to treat many-body interactions in semiconductors systematically using an electron-hole basis.[1,25–27] However, a cluster expansion is not employed in this work for two reasons. First, excitons are composite particles and there is no established method to expand higher-order exciton correlation functions (although some authors have proposed a possible solution recently[18,28]). Second, the dynamic equations with all the terms from the cluster expansion are prohibitively difficult to use in numerical simulations of complicated semiconductor systems such as BSSLs. Similarly, employing a higher-order DCT approach also generally leads to a large number of equations that are difficult to employ in complicated systems. Thus, to provide a tractable set of equations, in factorizing Eqs. (15) and (16) we employ precisely the RPA that is used to derive the SBEs. For example, we perform the following factorization:

$$\langle B_p^\dagger B_k^\dagger B_k \rangle = \langle B_p^\dagger \rangle \langle B_k^\dagger B_k \rangle (1 - \delta_{p,k}), \tag{17}$$

which uses the RPA to split the three-operator term into products of density and interband polarization.[10] In the fermionic basis, the above factorization amounts to

$$\langle B_p^\dagger B_k^\dagger B_k \rangle = \langle \alpha_p^\dagger \beta_{-p}^\dagger \alpha_k^\dagger \alpha_k \rangle \approx \langle \alpha_k^\dagger \alpha_k \rangle \langle \alpha_p^\dagger \beta_{-p}^\dagger \rangle. \tag{18}$$

This approach effectively groups together creation and annihilation operators with the same momentum whenever possible. For terms with four operators, the same RPA approach yields

$$\langle B_p^\dagger B_k^\dagger B_k B_q \rangle \approx \langle B_k^\dagger B_k \rangle \langle B_p^\dagger B_q \rangle (1 - \delta_{p,k})(1 - \delta_{k,q}). \quad (19)$$

The extra factors involving Kronecker delta functions in Eqs. (17) and (19) are included to ensure the condition of Eq. (8) is still satisfied after the factorization is applied.

The resulting dynamic equations are given by

$$
\begin{aligned}
i\hbar \frac{d}{dt}\langle B_p^\dagger \rangle = &- \sum_k \left[(E_g + V_0 + \epsilon_p^e + \epsilon_{-p}^h)\delta_{k,p} - V_{p-k} \right]\langle B_k^\dagger \rangle \\
&+ 2\sum_k V_{p-k}\langle B_p^\dagger \rangle\langle B_k^\dagger B_k \rangle - 2\sum_k V_{p-k}\langle B_k^\dagger \rangle\langle B_p^\dagger B_p \rangle \\
&+ \boldsymbol{\mathcal{E}}(t)\cdot \boldsymbol{M}_{cv} - 2\boldsymbol{\mathcal{E}}(t)\cdot \boldsymbol{M}_{cv}\langle B_p^\dagger B_p \rangle \\
&+ \left. i\hbar \frac{\partial}{\partial t}\langle B_p^\dagger \rangle \right|_{\text{scattering}}
\end{aligned}
\quad (20)
$$

and

$$
\begin{aligned}
i\hbar \frac{d}{dt}\langle B_p^\dagger B_q \rangle = &\sum_k V_{p-k}\langle B_k^\dagger B_q \rangle - \sum_k V_{q-k}\langle B_p^\dagger B_k \rangle + 2\sum_k \langle B_k^\dagger B_k \rangle (V_{p-k}\langle B_p^\dagger B_q \rangle - V_{q-k}\langle B_p^\dagger B_q \rangle)(1 - \delta_{p,k})(1 - \delta_{k,q}) \\
&- 2\sum_k V_{p-k}\langle B_p^\dagger B_p \rangle\langle B_k^\dagger B_q \rangle(1 - \delta_{p,k})(1 - \delta_{p,q}) + 2\sum_k V_{q-k}\langle B_q^\dagger B_q \rangle\langle B_p^\dagger B_k \rangle(1 - \delta_{p,q})(1 - \delta_{k,q}) + \boldsymbol{\mathcal{E}}(t)\cdot \boldsymbol{M}_{cv}\langle B_q \rangle \\
&- \boldsymbol{\mathcal{E}}^*(t)\cdot \boldsymbol{M}_{cv}^*\langle B_p^\dagger \rangle - 2\boldsymbol{\mathcal{E}}(t)\cdot \boldsymbol{M}_{cv}\langle B_p^\dagger B_p \rangle\langle B_q \rangle(1 - \delta_{p,q}) + 2\boldsymbol{\mathcal{E}}^*(t)\cdot \boldsymbol{M}_{cv}^*\langle B_p^\dagger \rangle\langle B_q^\dagger B_q \rangle(1 - \delta_{p,q}) + \left. i\hbar \frac{\partial}{\partial t}\langle B_p^\dagger B_q \rangle \right|_{\text{scattering}}.
\end{aligned}
\quad (21)
$$

In the above two equations, scattering induced dephasing and decay is included formally using the terms $i\hbar \frac{\partial}{\partial t}\langle B_p^\dagger \rangle|_{\text{scattering}}$ and $i\hbar \frac{\partial}{\partial t}\langle B_p^\dagger B_q \rangle|_{\text{scattering}}$. The exact causes of dephasing and decay are system dependent and can be dominated by carrier-phonon or carrier-carrier interactions depending on carrier density of the system. Such scattering could be described on various levels of sophistication. In this work, for simplicity, we will employ phenomenological time constants as this simplifies the discussion and the calculations and allows us to focus on the key issue of developing an excitonic alternative to the SBEs that includes PSF and exchange effects.

Equations (20) and (21) could be used directly to investigate carrier dynamics. These equations are like those obtained in the DCT approach[11,16] (but include higher-order terms that deal with PSF that were omitted in the particular version of DCT presented in Ref. 16). However, assuming a basis of m $\boldsymbol{k}$-states is required, there are $m(m+1)$ of the general qboson equations [we actually only need $m(m+3)/2$ equations since other equations can be found using complex conjugation]. In contrast, the SBEs consist of only $2m$ equations (or $3m$ if electron and hole populations are treated separately). Thus a calculation employing our qboson equations generally becomes prohibitive due to the fact that even for a one-dimensional (1D) system, hundreds of $\boldsymbol{k}$-states are generally required. Thus, we need to further simplify Eqs. (20) and (21) or transform them to a different basis. Our two approaches to transforming these equations are presented in Secs. III B and III C.

Before closing this section, we note that there are other possible ways to factorize the qboson dynamic equations. In particular, if biexcitonic effects are of interest, we could derive equations for $\langle B_p^\dagger B_q^\dagger \rangle$ and perform factorizations to retain terms related to biexcitons.[29,30] However, in this work our aim is to treat systems where intraband polarization plays a dominant role. Thus, we have chosen to obtain a group of equations that agree identically with SBEs in the coherent limit but that include important intraband correlations when we move out of the coherent limit.

B. Semiconductor Bloch equations

By making further approximations to Eqs. (20) and (21), we can reduce the number of equations and obtain a group of dynamic equations, which turns out to be just the SBEs. To accomplish this, we first note that Eq. (20) for $\langle B_p^\dagger \rangle$ only depends on $\langle B_k^\dagger \rangle$ and $\langle B_k^\dagger B_k \rangle$. From Eq. (21), the equation $\langle B_p^\dagger B_p \rangle$ is

$$
\begin{aligned}
i\hbar \frac{d}{dt}\langle B_p^\dagger B_p \rangle = &\sum_k V_{p-k}(\langle B_k^\dagger B_p \rangle - \langle B_p^\dagger B_k \rangle) + \boldsymbol{\mathcal{E}}(t)\cdot \boldsymbol{M}_{cv}\langle B_p \rangle \\
&- \boldsymbol{\mathcal{E}}^*(t)\cdot \boldsymbol{M}_{cv}^*\langle B_p^\dagger \rangle + \left. i\hbar \frac{\partial}{\partial t}\langle B_p^\dagger B_p \rangle \right|_{\text{scattering}}.
\end{aligned}
\quad (22)
$$

We note that Eq. (22) is much simpler than Eq. (21) because many terms disappear for $\boldsymbol{p} = \boldsymbol{q}$ either due to direct cancellation or due to δ functions. The problem now is that this equation contains intraband correlation functions $\langle B_p^\dagger B_k \rangle$, where $p \neq k$, and we have no dynamic equation for these. To make these equations closed, we choose the factorization

$$\langle B_p^\dagger B_q \rangle \approx \langle B_p^\dagger \rangle \langle B_q \rangle.$$

This factorization amounts to approximating intraband correlation functions by the product of two interband correlation functions and is precisely the factorization used in deriving the SBEs, where $\langle \alpha_p^\dagger \beta_{-k}^\dagger \beta_{-q} \alpha_q \rangle \approx \langle \alpha_p^\dagger \beta_{-k}^\dagger \rangle \langle \beta_{-q} \alpha_q \rangle$.[10] After this factorization, the two dynamic equations we obtain are Eq. (20) and

$$i\hbar \frac{d}{dt}\langle B_p^\dagger B_p \rangle = \sum_k V_{p-k}(\langle B_k^\dagger \rangle \langle B_p \rangle - \langle B_p^\dagger \rangle \langle B_k \rangle) + \boldsymbol{\mathcal{E}}(t) \cdot \boldsymbol{M}_{cv} \langle B_p \rangle$$
$$- \boldsymbol{\mathcal{E}}(t) \cdot \boldsymbol{M}_{cv}^* \langle B_p^\dagger \rangle + \left. i\hbar \frac{\partial}{\partial t}\langle B_p^\dagger B_p \rangle \right|_{\text{scattering}}. \quad (23)$$

Now to compare these equations directly with the SBEs, we make the following two standard definitions:[10]

$$P_p^* \equiv \langle B_p^\dagger \rangle, \quad (24)$$

$$n_{e,p} = n_{h,p} \equiv \langle B_p^\dagger B_p \rangle. \quad (25)$$

Using Eqs. (3) and (5), we see $P_p^* = \langle \alpha_p^\dagger \beta_{-p}^\dagger \rangle$ is the interband density matrix; $n_{e,p} = \langle \alpha_p^\dagger \alpha_p \rangle$ and $n_{h,p} = \langle \beta_p^\dagger \beta_p \rangle$ are the electron and hole occupation number for state $\boldsymbol{p}$. Using these definitions, we obtain from Eq. (20)

$$i\hbar \frac{d}{dt}P_p^* = -(E_g + \epsilon_p^e + \epsilon_{-p}^h)P_p^* + \sum_{k \neq p} V_{p-k}P_k^* + \sum_{k \neq p} V_{p-k}P_p^*(n_{e,k}$$
$$+ n_{h,k}) - (n_{e,p} + n_{h,p})\sum_{k \neq p} V_{p-k}P_k^* + \boldsymbol{\mathcal{E}}(t) \cdot \boldsymbol{M}_{cv}$$
$$- \boldsymbol{\mathcal{E}}(t) \cdot \boldsymbol{M}_{cv}(n_{e,p} + n_{h,p}) + \left. i\hbar \frac{\partial}{\partial t}\langle B_p^\dagger \rangle \right|_{\text{scattering}}. \quad (26)$$

Taking the complex conjugate and using the standard definitions

$$\hbar e_{e,p} \equiv \epsilon_p^e + E_g - \sum_{k \neq p} V_{p-k}n_{e,k}, \quad (27)$$

$$\hbar e_{h,p} \equiv \epsilon_p^h - \sum_{k \neq p} V_{p-k}n_{h,k}, \quad (28)$$

$$\omega_{R,p} \equiv \frac{1}{\hbar}\left[\boldsymbol{M}_{cv}^* \cdot \boldsymbol{\mathcal{E}}(t) + \sum_{k \neq p} V_{p-k}P_k \right], \quad (29)$$

where $\hbar e_{e,p}$ ($\hbar e_{h,p}$) is the renormalized single electron (hole) energy and $\omega_{R,p}$ is the generalized Rabi frequency, we obtain

$$\frac{d}{dt}P_p = -i(e_{e,p} + e_{h,p})P_p - i(n_{e,p} + n_{h,p} - 1)\omega_{R,p} - \frac{P_p}{T_{\text{inter}}^{\text{SBE}}}, \quad (30)$$

where we have introduced the time constant $T_{\text{inter}}^{\text{SBE}}$ to phenomenologically describe the interband decoherence due to various scattering processes. Equation (30) is the first of the standard SBE equations.

Now we turn to the second dynamic equation, Eq. (23). Using the above definitions, this equation becomes

$$i\hbar \frac{d}{dt}n_{e,p} = \sum_k V_{p-k}P_k^*P_p - \sum_k V_{q-k}P_p^*P_k + \boldsymbol{\mathcal{E}}(t) \cdot \boldsymbol{M}_{cv}P_p$$
$$- \boldsymbol{\mathcal{E}}(t) \cdot \boldsymbol{M}_{cv}^*P_p^* + \left. i\hbar \frac{\partial}{\partial t}\langle n_{e,p} \rangle \right|_{\text{scattering}}, \quad (31)$$

which can be further simplified to

$$\frac{d}{dt}n_{e,p} = -2\Im(\omega_{R,p}P_p^*) - \frac{n_{e,p}}{T_{\text{decay}}^{\text{SBE}}}, \quad (32)$$

where $T_{\text{decay}}^{\text{SBE}}$ is carrier decay time. An identical equation can be obtained for the hole populations, $n_{h,p}$. Equation (32) is the second of the standard SBE equations. Since the population scattering is being treated phenomenologically here, it would also be possible to assign different population decay constants to the electrons and holes (as is commonly done with the SBEs). In a system where there are many free carriers (as opposed to bound excitons), this freedom to assign different decay times may be important. In this work, for simplicity, we shall set these times equal. This is a good approximation when bound excitons are dominant; we discuss this further in Sec. IV D.

We close this section by noting that, in the SBE formalism, the interband polarization is given by

$$\boldsymbol{P}_{\text{inter}}(t) = \boldsymbol{M}_{cv}\sum_k \langle \alpha_k^\dagger \beta_{-k}^\dagger \rangle + \text{c.c.} = \boldsymbol{M}_{cv}\sum_k P_k^* + \text{c.c.} \quad (33)$$

There is no direct expression for the intraband polarization in the SBE formalism; however, the current density can be calculated from the carrier distributions using[31]

$$\boldsymbol{j}(t) = \frac{2e}{\hbar}\sum_k [n_{h,k}(t)\boldsymbol{\nabla}_k \epsilon_k^h - n_{e,k}(t)\boldsymbol{\nabla}_k \epsilon_k^e]. \quad (34)$$

C. Excitonic dynamic equations

The second approach to rendering Eqs. (20) and (21) more tractable is to transform them to a *true excitonic basis*. With such a transformation, we only need a basis of M true exciton states, where M may be much smaller than the number of $\boldsymbol{k}$ states, m, needed in the electron-hole basis approach. This reduction in the number of states required is a result of the fact that the excitonic states are the true two-particle states and thus are closer to eigenstates of an excited semiconductor at low to moderate densities. With a reduced number of equations in the true excitonic basis, it is no longer necessary to factorize $\langle B_p^\dagger B_q \rangle$ into the product of two interband terms, $\langle B_p^\dagger \rangle$ and $\langle B_q^\dagger \rangle$, in the calculation as was required in deriving the SBEs. This allows computational efficiency along with the key ability to retain intraband correlations. The equations derived in this section are the central result of this work.

In this approach, we use a basis of *true excitonic states*. These states have envelope functions, $\psi_\mu(\boldsymbol{r})$, which are the eigenstates of the exciton envelope-function Hamiltonian,

$$H^{\mathrm{ex}} = \frac{\boldsymbol{p}^2}{2m} + V(\boldsymbol{r}), \tag{35}$$

such that

$$H^{\mathrm{ex}}\psi_\mu(\boldsymbol{r}) = E_\mu \psi_\mu(\boldsymbol{r}). \tag{36}$$

Here, $m \equiv m_e^* m_h^* / (m_e^* + m_h^*)$ is the reduced mass, where m_e^* and m_h^* are the effective electron and hole masses, respectively, $\boldsymbol{r} = \boldsymbol{r}_e - \boldsymbol{r}_h$ is the electron-hole relative coordinate, $\boldsymbol{p}$ is the momentum conjugate to $\boldsymbol{r}$, $V(\boldsymbol{r})$ is the electron-hole interaction potential, and μ is the quantum number of the exciton with energy E_μ. We have not explicitly included any external potential, such as would arise from band discontinuities in nanostructures, but this can be included in our formalism.

The true exciton creation operator $B_\mu^\dagger$ is connected to qboson pair creation operators $B_k^\dagger$ through the canonical transformations,

$$B_\mu^\dagger = \sum_k c_\mu^k B_k^\dagger, \tag{37}$$

$$B_k^\dagger = \sum_\mu c_\mu^{k*} B_u^\dagger. \tag{38}$$

Here, c_μ^k is the coefficient of the exciton envelope function in the free electron-hole basis, i.e.,

$$\psi_\mu(\boldsymbol{r}) = \sum_k c_\mu^k f_k(\boldsymbol{r}), \tag{39}$$

where $f_k(\boldsymbol{r}) = \langle \boldsymbol{r} | \boldsymbol{k} \rangle = \frac{1}{\sqrt{V}} e^{i\boldsymbol{k}\cdot\boldsymbol{r}}$ is the free electron-hole envelope function.

We use the canonical transformation of Eq. (38) to derive the exciton dynamic equations from the qboson dynamic equations [Eqs. (20) and (21)]. We note that these two equations have been constructed so as to include the condition of Eq. (8) that prevents two qbosons from being in the same $\boldsymbol{k}$ state. Using Eqs. (37) and (38), Eq. (20) becomes

$$i\hbar \frac{d}{dt}\langle B_\mu^\dagger \rangle + E_\mu \langle B_\mu^\dagger \rangle = -i\hbar \frac{\langle B_\mu^\dagger \rangle}{T_{\mathrm{inter}}^{\mathrm{EXE}}}$$
$$+ 2 \sum_{\mu_1,\mu_2,\mu_3} R_{\mu_1,\mu_2,\mu_3}^\mu \langle B_{\mu_1}^\dagger \rangle \langle B_{\mu_2}^\dagger B_{\mu_3} \rangle$$
$$+ \boldsymbol{\mathcal{E}}(t) \cdot \boldsymbol{M}_{cv}^* \bigg(C_\mu$$
$$- 2 \sum_{\mu_1,\mu_2} C_{\mu,\mu_1,\mu_2} \langle B_{\mu_1}^\dagger B_{\mu_2} \rangle \bigg), \tag{40}$$

where

$$R_{\mu_1,\mu_2,\mu_3}^\mu = R1_{\mu_1,\mu_2,\mu_3}^\mu - R2_{\mu_1,\mu_2,\mu_3}^\mu, \tag{41}$$

$$R1_{\mu_1,\mu_2,\mu_3}^\mu = \sum_{k,p} V_{p-k} c_\mu^p c_{\mu_1}^{p*} c_{\mu_2}^{k*} c_{\mu_3}^k, \tag{42}$$

$$R2_{\mu_1,\mu_2,\mu_3}^\mu = \sum_{k,p} V_{p-k} c_\mu^p c_{\mu_2}^{p*} c_{\mu_1}^{k*} c_{\mu_3}^p, \tag{43}$$

$$C_\mu = \sum_p c_\mu^p = \psi_\mu(0), \tag{44}$$

$$C_{\mu,\mu_1,\mu_2} = \sum_p c_\mu^p c_{\mu_1}^{p*} c_{\mu_2}^p, \tag{45}$$

and $T_{\mathrm{inter}}^{\mathrm{EXE}}$ is the phenomenological interband dephasing time constant.

The second dynamic equation (21) after transformation becomes

$$i\hbar \frac{d}{dt}\langle B_\mu^\dagger B_\nu \rangle + (E_\mu - E_\nu)\langle B_\mu^\dagger B_\nu \rangle$$
$$= -i\hbar \langle B_\mu^\dagger B_\nu \rangle \left[\frac{1}{T_{\mathrm{intra}}^{\mathrm{EXE}}} + \delta_{\mu,\nu}\left(\frac{1}{T_{\mathrm{decay}}^{\mathrm{EXE}}} - \frac{1}{T_{\mathrm{intra}}^{\mathrm{EXE}}} \right) \right]$$
$$+ 2 \sum_{\mu_1,\mu_2,\mu_3,\mu_4} Z_{\mu_1,\mu_2,\mu_3,\mu_4}^{\mu,\nu} \langle B_{\mu_1}^\dagger B_{\mu_4} \rangle \langle B_{\mu_2}^\dagger B_{\mu_3} \rangle$$
$$+ [\boldsymbol{\mathcal{E}}(t) \cdot \boldsymbol{M}_{cv}^* C_\mu \langle B_\nu \rangle - \boldsymbol{\mathcal{E}}^*(t) \cdot \boldsymbol{M}_{cv} C_\nu^* \langle B_\mu^\dagger \rangle]$$
$$- 2 \sum_{\mu_1,\mu_2,\mu_3} [\boldsymbol{\mathcal{E}}(t) \cdot \boldsymbol{M}_{cv}^* U_{\mu_1,\mu_2,\mu_3}^{\mu,\nu} \langle B_{\mu_1}^\dagger B_{\mu_2} \rangle \langle B_{\mu_3} \rangle$$
$$- \boldsymbol{\mathcal{E}}(t) \cdot \boldsymbol{M}_{cv} U_{\mu_3,\mu_2,\mu_1}^{\nu,\mu*} \langle B_{\mu_1}^\dagger \rangle \langle B_{\mu_2}^\dagger B_{\mu_3} \rangle], \tag{46}$$

where

$$Z_{\mu_1,\mu_2,\mu_3,\mu_4}^{\mu,\nu} = S_{\mu_1,\mu_2,\mu_3,\mu_4}^{\mu,\nu} - T_{\mu_1,\mu_2,\mu_3,\mu_4}^{\mu,\nu}, \tag{47}$$

$$S_{\mu_1,\mu_2,\mu_3,\mu_4}^{\mu,\nu} = \sum_{k,p,q} (V_{p-k} - V_{q-k})(1 - \delta_{p,k})$$
$$\times (1 - \delta_{k,q}) c_\mu^p c_\nu^{q*} c_{\mu_1}^{p*} c_{\mu_2}^{k*} c_{\mu_3}^k c_{\mu_4}^q, \tag{48}$$

$$T_{\mu_1,\mu_2,\mu_3,\mu_4}^{\mu,\nu} = \sum_{k,p,q} (c_\mu^p c_\nu^{q*} V_{k-p} - c_\mu^k c_\nu^{p*} V_{q-p})(1 - \delta_{p,k})$$
$$\times (1 - \delta_{p,q}) c_{\mu_1}^{k*} c_{\mu_2}^{p*} c_{\mu_3}^p c_{\mu_4}^q, \tag{49}$$

$$U_{\mu_1,\mu_2,\mu_3}^{\mu,\nu} = \sum_{p,q} c_\mu^p c_\nu^{q*} c_{\mu_1}^{p*} c_{\mu_2}^p c_{\mu_3}^q (1 - \delta_{p,q}). \tag{50}$$

In Eq. (46), the dephasing of intraband correlation functions ($\langle B_\mu^\dagger B_\nu \rangle$ where $\mu \neq \nu$) is included phenomenologically via the intraband dephasing time constant $T_{\mathrm{intra}}^{\mathrm{EXE}}$, while decay of the exciton populations ($\langle B_\mu^\dagger B_\mu \rangle$) is accounted for via the decay time constant, $T_{\mathrm{decay}}^{\mathrm{EXE}}$.

We note that in the EXEs, although we cannot introduce different decay times for electron and hole populations as one could with the SBEs, we can specify the interband dephasing, intraband dephasing, and population decay time constants independently. For systems where intraband dynamics are important and bound excitons dominate, this flexibility is more important than having different decay times for electrons and holes.[16]

The EXEs satisfy a number of important properties. In particular, as is shown in Sec. IV C and Appendix A, once the optical pulse is gone, the total carrier number and total energy are both conserved when the dephasing and decay time constants are set to infinity. This is a property that is not

obeyed in general by approaches that are perturbative in the optical field.

In our derivation of the EXEs, we have chosen to transform the pair-space dynamic equations. Another possible approach would be to transform the pair-space Hamiltonian of Eq. (11) into an excitonic basis, and then use the Heisenberg equations of motion to derive the EXEs. However, it can be easily shown that such an approach leads to incorrect dynamic equations unless great care is taken to also apply Eq. (8). The problem is that the dynamic equations for $B_\mu^\dagger$ and $B_\mu^\dagger B_\nu^\dagger$ that are derived directly from this exciton Hamiltonian also contain terms with products such as $B_{\mu_1}^\dagger B_{\mu_2}^\dagger$ and $B_{\mu_1} B_{\mu_2}$; unless extreme care is taken, portions of these terms will contain products $B_k^\dagger B_k^\dagger$ or $B_k B_k$ (from the expansions of $B_{\mu_1}^\dagger B_{\mu_2}^\dagger$) that have coefficients that are nonzero. Unless one uses Eq. (8) to explicitly remove the nonphysical terms, the resulting equations are incorrect. In practice, it is much simpler to derive the equations of motion in the qboson pair space first and then transform the equations to the exciton basis while enforcing the condition $B_k^\dagger B_k^\dagger = 0$. This is the approach we have used in this section. We note that this result implies that it is not possible to derive an exciton Hamiltonian from which the equations of motion can be determined using only the commutation relations. This is consistent with the findings of Combsecot and Betbeder-Matibet.[20]

We close this section by noting that, in the excitonic basis, the interband polarization is given by

$$\boldsymbol{P}_{\text{inter}}(t) = \sum_k \boldsymbol{M}_{cv}\langle B_k^\dagger \rangle + \text{c.c.} = \sum_\mu \boldsymbol{M}_\mu \langle B_\mu^\dagger \rangle + \text{c.c.}, \quad (51)$$

where $\boldsymbol{M}_\mu = \boldsymbol{M}_{cv}\psi_\mu(r=0)L^{d/2}$ is the exciton interband dipole matrix element; d and L are the dimension and length of the system. In the excitonic basis, the intraband polarization is given by[15]

$$\boldsymbol{P}_{\text{intra}}(t) = \frac{1}{V}\sum_{\mu,\nu} \boldsymbol{G}_{\mu,\nu}\langle B_\mu^\dagger B_\nu \rangle,$$

where $\boldsymbol{G}_{\mu,\nu}$ is the intraband dipole matrix elements between two excitonic states $|\psi_\mu\rangle$ and $|\psi_\nu\rangle$ that is given by

$$\boldsymbol{G}_{\mu\nu} = \langle \psi_\mu | -e(\boldsymbol{r}_e - \boldsymbol{r}_h)|\psi_\nu\rangle.$$

The current density is given simply by the time derivative of $\boldsymbol{P}_{\text{intra}}(t)$.

IV. RESULTS AND DISCUSSION

In this section, we present the results of simulations obtained using our EXEs and compare them to results using the SBEs. We present the interband polarization spectra obtained using both the EXEs and the SBEs. We show that the two approaches yield almost identical results when we are in the coherent limit but differ significantly when we move to more general dephasing situations. We then present the temporal evolution of exciton population, and show how the blueshift in interband polarization spectra can be understood as arising from the PSF-induced exciton population redistribution. Finally, we discuss the differences between the EXEs and the

SBEs and the conditions under which our EXEs are expected to have significant advantages.

A. Model system

Our model system is a 1D quantum wire of length L with periodic boundary condition. We treat the electron-hole interaction as a contact potential

$$V(\boldsymbol{r}) = -A\,\delta(\boldsymbol{r}), \quad (52)$$

where $A > 0$. This simplified interaction has been used by previous authors to model the interband optical spectra of nanoring magnetoexcitons[32] and investigate intraband dynamics.[16] With this potential, there is a single bound excitonic state and a quasicontinuum of unbound excitonic states. We choose this system because it is a simple system in which both the EXEs and SBEs can be implemented. Although, unlike in a BSSL, there is no macroscopic intraband polarization and thus intraband effects are relatively modest in this system, we find that the effects are large enough to clearly see the differences between the two approaches.

In all that follows, we take the unit of length to be $r_B = 2\hbar^2/mA$, which is the Bohr radius of our bound 1D exciton, where m is the mass of an electron or hole (taken to be the same in our model for simplicity). The energy unit is the binding energy of the bound exciton, which is $E_b = mA^2/4\hbar^2 = A/2r_B$. The time unit is $\tau_0 \equiv \hbar/E_b = 4\hbar^3/mA^2$.

We choose our parameters so as to approximately model a GaAs nanoring excited via an ultrashort laser pulse. We take the length of the model system to be $L=50r_B$ so that the system can hold several excitons before PSF effects become significant. The binding energy of a bound exciton in such a system is on the order of 10 meV. Since a typical energy gap between the valence and conduction band is on the order of 1 eV, we set $E_g = 100E_b$ in our model system. These conditions yield $E_b = 10$ meV, $r_B \approx 1.34$ nm, and $\tau_0 \approx 65.91$ fs.

The laser pulse electric field is given by

$$\boldsymbol{\mathcal{E}}(t) = \boldsymbol{E}_0 e^{-i\omega_c t - t^2/\tau_p^2} + \text{c.c.}, \quad (53)$$

which is a transform-limited Gaussian pulse centered at frequency ω_c. Thus, the pulse intensity is

$$S(t) = I\exp(-2t^2/\tau_p^2)$$

and the spectral power density is

$$\bar{S}(\omega) = \pi I\tau_p^2 \exp[-(\omega-\omega_c)^2\tau_p^2/2],$$

where I is the peak intensity. The central frequency of the pulse is set to be resonant with the ($\mu=0$) ground excitonic state, i.e., $\hbar\omega_c = E_0 = E_g - E_b$. In addition, the spectra width of the pulse is narrow enough such that at low intensities, the vast majority of the excitons are excited directly into the ground state with very few unbound excitons created. This requirement is satisfied by choosing the temporal width of the laser pulse to be $\tau_p = 1.875\tau_0$, which corresponds to approximately 120 fs. Figure 1 shows the spectral density of the laser pulse that is used in all the simulations, along with the calculated discrete excitonic energy levels for the first 28 excitonic states. In all calculations we employ the usual ro-
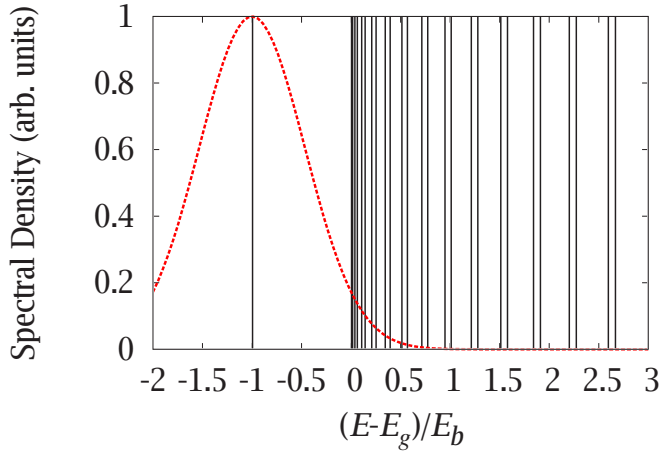
FIG. 1. (Color online) The spectral density of the laser pulse (red dotted line) is shown along with the discrete exciton energy levels from $\mu=0$ (the bound exciton level) up to $\mu=26$.
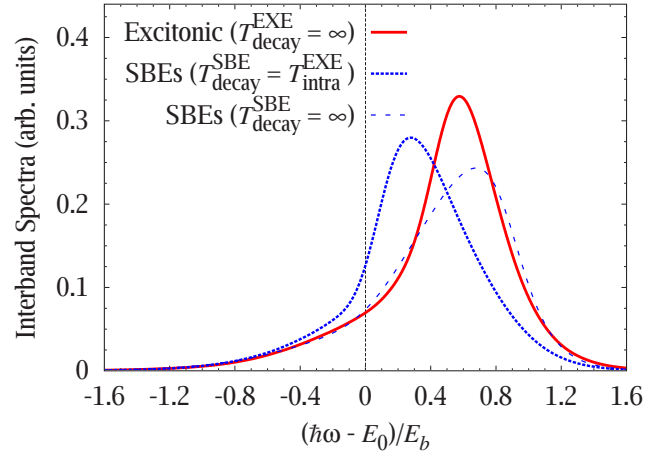

FIG. 2. (Color online) The spectral density of the interband polarization calculated using the SBEs and EXEs. In the EXE result (red solid line), $T_{\text{decay}}^{\text{EXE}}=\infty$ and $T_{\text{intra}}^{\text{EXE}}=1.5T_{\text{inter}}$. In one of the SBE results (blue dotted line), $T_{\text{decay}}^{\text{SBE}}=T_{\text{intra}}^{\text{EXE}}=1.5T_{\text{inter}}$, while in the other (blue dashed line) $T_{\text{decay}}^{\text{SBE}}=T_{\text{decay}}^{\text{EXE}}=\infty$.

tating wave approximation for the optical field.[10]

In our model system, there is only one bound excitonic state ($\mu=0$) and it is well separated in energy from the other states. The unbound quasicontinuum excitonic states generally come in pairs of symmetric and antisymmetric states (see Fig. 1). The symmetric states ($\mu=1,3,5,\ldots$) are optically active, while the antisymmetric ones ($\mu=2,4,6,\ldots$) are optically forbidden. However, it is necessary to include the antisymmetric states, because as we shall see, when PSF effects are included, they can become populated and thereby affect the dynamics of the optically active states.

B. Interband polarization simulations

Ultrafast carrier dynamics in semiconductors is an intrinsic many-body problem. As carrier density increases, many-body interactions become increasingly more important. To emphasize the PSF and exchange effects, we use a relatively high pulse intensity that creates high carrier densities in the system. At such densities, there are other higher-order many-body effects that may be important that are omitted in both the EXEs and the SBEs. However, we operate at these densities because our goal is to clearly demonstrate the near equivalence of the two approaches in the coherent limit and to examine the effects of the different treatments of intraband coherences. Our results make it evident that the treatment of *intraband* polarization dephasing should be treated with care as it can have a strong influence on the *interband* spectra.

In Fig. 2, we present the interband polarization spectral density at a relatively high laser intensity that gives rise to a relatively high exciton (carrier) density. Once the pulse has passed, the ratio of the density radius, $r_s=L/N$, to the exciton Bohr radius, r_B, is $r_s/r_B\approx3.5$, where N is the total number of excitons (bound and unbound). To compare the two approaches, we show the EXE result along with two different SBE results. Because the interband dephasing time describes the same process in the SBEs as in the EXEs, we set the SBE interband polarization dephasing time, $T_{\text{inter}}^{\text{EXE}}$, to be equal to the EXE interband dephasing time, $T_{\text{inter}}^{\text{EXE}}$, and denote both simply by T_{inter} from here on.

In the EXE calculation, we have three time constants: T_{inter}, $T_{\text{intra}}^{\text{EXE}}$, and the excitonic population decay time, $T_{\text{decay}}^{\text{EXE}}$. For both the EXE and SBE calculations, the interband dephasing time constant is taken to be $T_{\text{inter}}=3.75\tau_0$, which corresponds to 247 fs. The precise choice of this time constant does not qualitatively change our results; it has been chosen to be in the range of those seen in semiconductor nanostructures at low temperature.[8] The EXE intraband dephasing time, $T_{\text{intra}}^{\text{EXE}}$, is chosen to follow the relation $T_{\text{intra}}^{\text{EXE}}=1.5T_{\text{inter}}$ that has been shown to be approximately valid experimentally[33] and theoretically[34] in BSSLs. Finally, because, in experiments, the exciton population decay time is generally much longer than either dephasing time, we set $T_{\text{decay}}^{\text{EXE}}=\infty$ in our calculation. At low intensities, the interband spectrum is simply a Lorentzian line centered about $\hbar\omega=E_0$. Thus, we see that for this system, PSF and exchange result in a significant blueshift in the spectrum. As we discuss in Sec. IV C, this blueshift can be understood as arising from a driving of excitons to higher-energy states.

In the SBE calculation, the intraband and interband dephasing times cannot be specified separately and there are only two time constants: the interband dephasing time, T_{inter}, and the carrier decay time, $T_{\text{decay}}^{\text{SBE}}$. There is no clear choice for $T_{\text{decay}}^{\text{SBE}}$ as it effectively describes population decay as well as part of the intraband dephasing. In fact, as has been shown by Axt *et al.*,[16] the intraband dephasing in the SBEs is determined both by $T_{\text{decay}}^{\text{SBE}}$ and $T_{\text{inter}}/2$ and so cannot be fully controlled independently of T_{inter}. To facilitate comparison of the SBE and EXE results, we present the SBE results both with $T_{\text{decay}}^{\text{SBE}}=T_{\text{decay}}^{\text{EXE}}=\infty$ and $T_{\text{decay}}^{\text{SBE}}=T_{\text{intra}}^{\text{EXE}}=1.5T_{\text{inter}}$. As can be clearly seen, neither of the SBE results agrees at all well with the EXE results.

We note that in our numerical simulations both for the SBEs and the EXEs, we have increased the basis size until convergence has been reached to better than 4%. For the SBEs, this meant using a basis of 500 states. For the EXEs,

this required a basis of 100 states at this intensity. The details of the convergence properties of the EXEs for this system are discussed in Appendix B.

The main differences between the SBE and EXE results arise from the inability of the SBEs to treat intraband dephasing correctly. From our EXE results, we find that both the intraband correlation functions and carrier populations can strongly affect the evolution of the carrier distributions amongst energy states, which in turn affects the interband spectrum. Thus, the way in which intraband dephasing is treated can have a very significant effect on the interband spectra.

The effects of intraband and decay time constants can be better understood via an inspection of the second dynamic equation in both formalisms, Eqs. (32) and (46). In the SBEs, there are three terms that can change carrier distribution,

$$\frac{dn_{e,p}}{dt} = -\frac{2}{\hbar}\Im[\boldsymbol{M}_{cv}^* \cdot \boldsymbol{\mathcal{E}}(t)P_p^*] - \frac{n_{e,p}}{T_{\text{decay}}^{\text{SBE}}} - \frac{2}{\hbar}\Im\left[\left(\sum_{k \neq p} V_{k-p}P_k\right)P_p^*\right],$$

(54)

where the product $P_k P_p^*$ is obtained by factorizing an intra-band correlation term. In the true exciton space, as can be seen from Eq. (46), there are many terms that can potentially change the carrier distribution. Things become clearer if we transform Eq. (46) from the true exciton basis back to the qboson pair-space basis. Doing this, we obtain

$$\frac{d}{dt}\langle B_p^\dagger B_p \rangle = -\frac{2}{\hbar}\Im(\boldsymbol{M}_{cv}^* \cdot \boldsymbol{\mathcal{E}}(t)\langle B_p^\dagger \rangle) - \frac{\langle B_p^\dagger B_p \rangle}{T_{\text{intra}}^{\text{EXE}}}$$

$$- \frac{2}{\hbar}\Im\left(\sum_{k \neq p} V_{k-p}\langle B_p^\dagger B_k \rangle\right)$$

$$+ \left(\frac{1}{T_{\text{decay}}^{\text{EXE}}} - \frac{1}{T_{\text{intra}}^{\text{EXE}}}\right)\sum_{k,q} F_{p,k,q}\langle B_k^\dagger B_q \rangle, \quad (55)$$

where $F_{p,k,q} \equiv \Sigma_\mu c_\mu^{p*} c_\mu^p c_\mu^k c_\mu^{q*}$. Comparing Eq. (55) to Eq. (54), we see that the first two terms are identical in the two equations. The third terms are the same apart from the factorization (which we will return to shortly). However, the fourth term in Eq. (55) is not found in Eq. (54) and is nonzero unless we set $T_{\text{decay}}^{\text{EXE}} = T_{\text{intra}}^{\text{EXE}}$. This additional term is determined by the difference between intraband dephasing and population decay time constants. Thus, if $T_{\text{decay}}^{\text{EXE}} = \infty$, while $T_{\text{intra}}^{\text{EXE}} = 1.5T_{\text{inter}}$, this extra term is a major cause of the differences between the EXE and the SBE results. To show the effect of this term, in Fig. 3(a) we plot the results for the EXE and SBE with $T_{\text{intra}}^{\text{EXE}} = T_{\text{decay}}^{\text{EXE}} = T_{\text{decay}}^{\text{SBE}} = 1.5T_{\text{inter}}$. This removes the difference caused by the fourth term in Eq. (55) and thereby makes the SBE and EXE results much closer; however, they are still significantly different.

A second important difference between Eqs. (54) and (55) lies in the third term in each equation. We have shown that it is necessary to factorize $\langle B_p^\dagger B_k \rangle$ to obtain SBEs from equations derived in the EXE. This factorization has a potential problem in that $\langle B_p^\dagger B_k \rangle$ is not necessarily equal to $\langle B_p^\dagger \rangle \langle B_k \rangle$, especially when intraband polarization dominates the optical
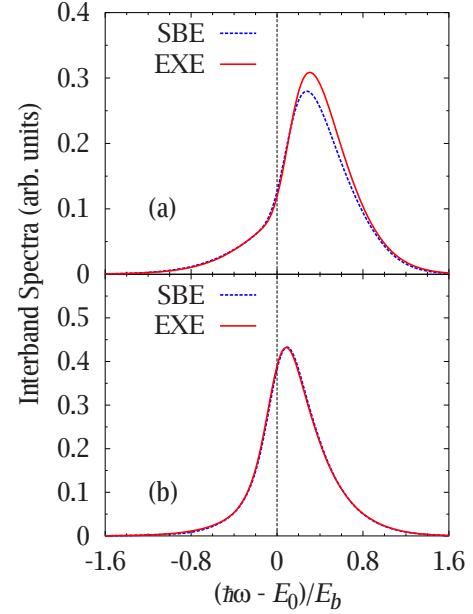

FIG. 3. (Color online) The spectral density of the interband polarization calculated using the SBEs and EXEs. In (a) $T_{\text{decay}}^{\text{SBE}} = T_{\text{decay}}^{\text{EXE}} = T_{\text{intra}}^{\text{EXE}} = 1.5T_{\text{inter}}$ is used, while in (b) the coherent limit condition $T_{\text{decay}}^{\text{SBE}} = T_{\text{decay}}^{\text{EXE}} = T_{\text{intra}}^{\text{EXE}} = T_{\text{inter}}/2$ is used.

response of the system or is, in fact, driven by an external terahertz field.[14,16] In any system (such as the one considered here), these two types of terms will strongly differ at later times unless the time constants are in the coherent limit condition: $T_{\text{intra}}^{\text{EXE}} = 0.5T_{\text{inter}}$. This is because $\langle B_p^\dagger \rangle \langle B_k \rangle = P_k P_p^*$ has a decoherence time constant of $0.5T_{\text{inter}}$ while $\langle B_p^\dagger B_k \rangle$ has a decoherence time constant of $T_{\text{intra}}^{\text{EXE}}$. To show the effect of being in the coherent limit, in Fig. 3(b) we present the results of the SBE and EXE calculations when we force the coherent limit by setting $T_{\text{decay}}^{\text{EXE}} = T_{\text{intra}}^{\text{EXE}} = T_{\text{decay}}^{\text{SBE}} = 0.5T_{\text{inter}}$. In this special case the two results are almost indistinguishable, indicating that in the coherent limit our EXEs produce results that are almost identical to the SBEs for this system. We note that because the carrier decay time used in Fig. 3(b) is much shorter than that used in Fig. 3(a) or Fig. 2 the blueshift is much smaller. This is because those terms related to intraband correlation functions in Eq. (40) have less of an effect due to their faster decay or dephasing.

Even though the EXE and SBE results plotted in Fig. 3(b) appear to be almost identical, there are, in principle, small differences between the two results. This is because, even in the coherent limit, the two equations are still not identical due to the factorization of intraband correlation functions used to derive the SBEs. To demonstrate this, we define the difference correlation function given by the difference between the factorized and unfactorized intraband correlation functions: $A_{p,q} \equiv \langle B_p^\dagger B_q \rangle - \langle B_p^\dagger \rangle \langle B_q \rangle$. If we replace the products $P_k^* P_p$ in Eq. (31) by $P_p^* P_q + A_{p,q}$ we recover the unfactorized Eq. (22). Using Eqs. (20) and (21), we find that the equation of motion for $A_{p,q}$ ($p \neq q$) is
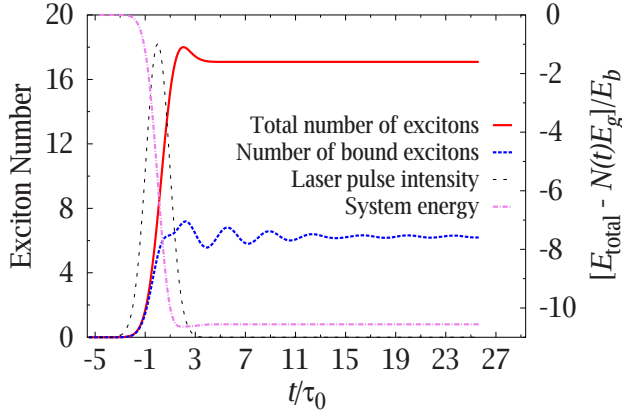
FIG. 4. (Color online) Temporal evolution of total number of excitons (red solid line), number of excitons in the bound state (blue dashed line), and the system energy, $E_{\text{total}} - N(t)E_g$ (violet dash-dotted line). In the calculations, the interband and intraband dephasing times and the population decay time are all set to infinity. For reference, the laser pulse intensity is also plotted.

FIG. 5. Exciton population, N_μ, of the μth excitonic state as a function of time and excitonic state number, μ. Note that the ground state exciton population ($N_0 \approx 6$) is not shown in this figure but is given in Fig. 4.

$$i\hbar \frac{d}{dt} A_{p,q} = \sum_k V_{p-k} A_{k,q} - \sum_k V_{q-k} A_{p,k} - 2 \sum_k V_{p-k} A_{k,q} \langle B_p^\dagger B_p \rangle$$
$$+ 2 \sum_k V_{q-k} \langle B_q^\dagger B_q \rangle A_{p,k} + 2 \sum_k V_{p-k} \langle B_k^\dagger B_k \rangle A_{p,q}$$
$$- 2 \sum_k \langle B_k^\dagger B_k \rangle A_{p,q} V_{q-k}$$
$$- 2(\langle B_q^\dagger B_q \rangle - \langle B_p^\dagger B_p \rangle) \langle B_p^\dagger B_q \rangle V_{p-q}.$$

The last term in this equation, which is fourth order in the optical field, is the only source term for $A_{p,q}$. Thus, in the coherent limit, the difference between the population distributions for the SBEs and the EXEs is at least fourth order in the optical field and so the difference between the interband polarization is at least fifth order in the optical field. For the system and intensities considered here, this difference appears to be negligible, as shown in Fig. 3(b). However, there is no guarantee that this will be the case for all systems.

To summarize the results of this section, we have shown that if we operate in the coherent limit, our EXEs are identical to the SBEs to at least third order in the optical field. However, if the dephasing times do not obey the coherent limit condition that $T_{\text{decay}}^{\text{EXE}} = T_{\text{intra}}^{\text{EXE}} = T_{\text{decay}}^{\text{SBE}} = 0.5 T_{\text{inter}}$, then we obtain significantly different results using our EXEs. Furthermore, if the exciton population decay time differs significantly from the exciton intraband dephasing time (as is generally expected), then the differences are even larger.

C. Exciton population dynamics

Having compared the results of the EXEs to the SBEs in the previous section, in this section we examine how the observed spectral blueshift and other aspects of the optical response can be largely understood by examining the exciton population dynamics. In Figs. 4 and 5 we present the total number of excitons and the exciton population distribution,
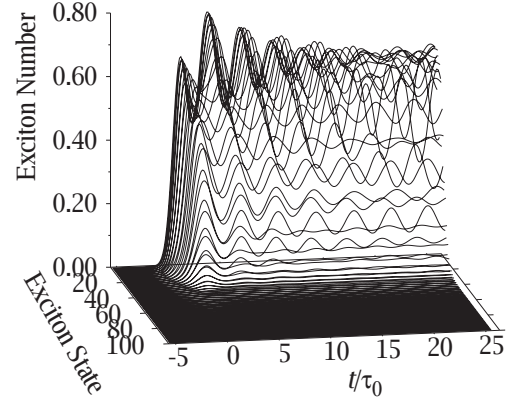
respectively, as a function of time for the same laser intensity used to produce Figs. 2 and 3. To simplify discussion, in these calculations we have not included dephasing or population decay, i.e., we set $T_{\text{inter}} = T_{\text{intra}}^{\text{EXE}} = T_{\text{decay}}^{\text{EXE}} = \infty$.

The total exciton population is given by $N \equiv \langle \hat{N} \rangle$, where

$$\hat{N} \equiv OU \left(\sum_k \alpha_k^\dagger \alpha_k \right) U^\dagger O^\dagger = \sum_k B_k^\dagger B_k = \sum_\mu B_\mu^\dagger B_\mu \quad (56)$$

is the *total exciton number operator*. In addition, the number of excitons in the μth excitonic state is given simply by $N_\mu \equiv \langle B_\mu^\dagger B_\mu \rangle$. From Fig. 4 we see that, as expected, the total exciton population is constant once the optical pulse has passed. This is one of the key features of our excitonic equations (see Appendix A). From Fig. 4, we can also see that the EXEs conserve energy too, as one would hope [note that we have subtracted the quantity $N(t)E_g$ in the energy plot in Fig. 4 from the total energy]. This result can also be proven analytically (see Appendix A). However, from both Figs. 4 and 5 we see that although the total exciton population is constant after the pulse has passed, the populations N_μ of individual excitonic states are oscillating strongly in time. These population oscillations are due entirely to PSF effects, which introduce coupling between the excitonic states. These oscillations are essentially beating effects that arise because, due to many-body interactions, the excitonic state, ψ_μ, is not an eigenstate of the system except when $N=1$. Thus, the number of excitons in a given eigenstate is not a good quantum number (whereas the total number of excitons is, once the pulse has passed). For ground state excitons, the period of the oscillation is approximately determined by the energy difference, E_b, between exciton ground state and lowest continuum state, as expected. From Figs. 4 and 5 it is also clear why the interband polarization is blueshifted: due to PSF (particularly the hole-burning terms), a large fraction of the excitons in the system are effectively created in excited states and not the ground state. As a result, the interband polarization is blueshifted towards the energies of those excited states.

Another interesting feature exhibited in Fig. 5 is that the antisymmetric exciton states ($\mu=2,4,6,\ldots$), which are optically forbidden in the linear regime, are strongly populated at these high intensities. This effect can be understood by analyzing the nonlinear terms in Eq. (46) that are caused by PSF. After including these nonlinear terms, it turns out that the *effective* oscillator strengths of the antisymmetric states are no longer zero.

D. Comparison of excitonic equation and semiconductor Bloch equation approaches

In the previous section (Sec. IV B), we simulated the interband response of a nanoring. This system was chosen not because it is the most suitable one for displaying the advantages of an excitonic approach, but rather because it can be simulated relatively easily using either the SBE or the EXE approach, thereby allowing a direct comparison of the two approaches. The question that we address in this section is the following: Which systems would be better treated using the EXEs than the SBEs and vice versa?

The SBEs and the EXEs have a number of characteristics in common. They both allow the treatment of PSF and exchange in the RPA in a manner that is nonperturbative in the optical field. Both of the approaches are computationally efficient, which allows for the treatment of complicated systems. They both allow for the inclusion of dephasing and decay effects phenomenologically and both systems of equations can be extended to include other effects such as dynamic screening (see, e.g., Ref. 8 for EXEs) and carrier-phonon scattering (see, e.g., Ref. 34 for EXEs).

Although both approaches have much in common, as we saw in the previous section, the results obtained using the two approaches can differ significantly under certain circumstances. The key difference between the two approaches lies in their treatment of dephasing, decoherence, and decay effects. Because the basis used in the two approaches is different, the meaning of a population and an intraband coherence is different in the two bases. If the SBE and EXE interband dephasing times are taken to be independent of k and μ, respectively, then the interband dephasing is equivalent in the two systems. However, the population decay time in the SBEs refers to electron and hole populations, whereas in the EXEs it refers to exciton populations. A consequence of this, for example, is that what is seen as a pure electron-hole population in the SBE basis is found to include intraband correlations between different excitonic states in the EXE approach. In addition, using the EXEs it is possible to specify separately an intraband dephasing time and a population decay time and thus separate two rather different effects. As is discussed in the previous section, these key differences between the two approaches give rise to different results for the interband polarization spectra.

When bound excitons dominate the response, then it is preferable to employ an excitonic basis and our EXEs will generally be more accurate than the SBEs. This is because excitons are closer to being the eigenstates of the semiconductor system than the uncorrelated electron and hole states. This difference will be important even if one moves beyond

a phenomenological treatment of scattering. For example, in the usual treatment of carrier-phonon scattering, one usually has to make the Markov approximation, and it has been shown by Hader *et al.*[35] that the closer the scattering states are to the eigenstates of the system, the more accurate the results are.

When free (unbound) carriers dominate the response, then an electron-hole basis is likely preferable. In this case, the SBEs are expected to be more accurate than the EXEs *as long as the system is in the coherent limit*. Thus the SBEs may perform very well for excitation in bulk or quantum wells at energies considerably above the bound exciton energy. The SBEs have the advantage that they allow the electron and hole scattering to be treated separately, which is important if there are large numbers of free carriers and the electron and hole scattering times are very different. A second advantage of the SBEs is that they can be more easily generalized than the EXEs to allow for more general treatments of carrier-carrier scattering beyond phenomenological dephasing and decay. In fact, they can be thought of as the first order results in a more general cluster expansion approach. If the system is sufficiently simple, then such higher-order approaches (as well as DCT) can be applied. However, in complicated systems such as a BSSL, computational complexity generally limits one to employ either the SBEs or EXEs.

From the above discussion, we see that the EXE approach will generally perform better than the SBEs when either of the following two conditions are met: (1) the response is dominated by bound excitons and/or (2) there is a sizable macroscopic intraband polarization in the system. As an example, one important system that meets both these criteria is a BSSL excited by a short optical pulse centered spectrally below the $n=0$ $1s$ exciton WSL level (see Introduction). The pulse excites primarily $1s$-like excitons and induces intraband correlations between these excitonic states that result in terahertz emission at the Bloch-oscillation frequency. Because the EXEs include intraband excitonic correlations naturally, they do very well in treating this system.[14,15] In contrast, the terahertz emission calculated using the SBEs is incorrect unless the system is in the coherent limit. Because the intraband polarization in a BSSL can also affect the *interband* response,[13] the SBEs will also fail to treat the interband polarization correctly beyond first order in the optical field.

In the previous section, we presented results at high pulse intensities to emphasize the PSF effects and to aid in comparison of the SBEs with the EXEs. As we saw, the SBEs had clear deficiencies when we were not in the coherent limit. On the other hand, at these intensities, a large fraction of the carriers generated were *unbound* excitons (see Fig. 5); thus the EXE approach may also encounter difficulties if the electron and hole scattering times are very different. Thus, for this system, the preferred approach will depend on the nature of the actual dephasing in the system and the pulse intensity used. This is the general situation: whether the EXEs are preferable to the SBEs will depend on the details of the various scattering times and processes, the pulse intensity and frequency, and the particular system being excited. However, because the EXE approach allows us to cal-

culate the excitonic population distributions, it enables us to clearly evaluate the relative contributions of bound and unbound excitons and thereby determine whether the EXE approach is the preferred choice.

V. CONCLUSION

In this work, we have presented an excitonic formalism for treating the ultrafast nonlinear response of semiconductors. Our approach goes beyond most existing excitonic models by including PSF and exchange and thereby provides an alternative to the SBEs. Using a simple model system, we have demonstrated that our excitonic model is identical to the SBEs to third order in the optical field if the dephasing is such that one is working in the coherent limit. We showed, however, that if one moves away from the coherent limit then there are significant differences between results obtained with this excitonic approach and the SBEs. These differences are mainly caused by differences in the treatment of intraband coherences in the system. Because of its ability to treat intraband polarization without factorization, our excitonic approach has potential advantages in systems where the intraband response is important (for determining either terahertz or optical emission). In addition, because our excitonic approach treats intraexcitonic coherences exactly, it also has advantages over the SBEs in treating systems where bound excitons dominate the optical or terahertz response.

In addition to enabling the calculation of the interband or intraband response of a system, this excitonic formalism also provides details of the population dynamics of bound and unbound excitonic states, thereby providing different insight into the nonlinear optical response of a given semiconductor system.

Although we have largely compared our excitonic approach to the SBEs, there are of course other more sophisticated, higher-order approaches to treating ultrafast dynamics, such as cluster expansions and DCT. These approaches will generally provide more accurate modeling of the response than either the SBEs or EXEs. In particular, DCT is able to include intraband correlations in a similar manner to our EXEs. However, because they rely on the use of a large free-carrier basis, in contrast to our EXEs, they may not be practical in complicated systems, such as BSSLs.

In this paper, we have applied our EXEs to treat a simple model of a nanoring. However, these equations should be suitable for the investigation of exciton dynamics in a wide range of systems, such as quantum wells and BSSLs. In such systems they could be used to calculate the intraband polarization (and emitted terahertz radiation) and to investigate transitions between different exciton states that are induced by an external terahertz pulse. The main difficulty with our excitonic approach is that as the carrier density is increased, so will the number of excitonic states required to treat PSF. The task in treating more complex systems is thus to determine which and how many states must be included for an accurate treatment of these effects. This is the subject of future work.

APPENDIX A: CONSERVATION OF TOTAL EXCITON POPULATION AND ENERGY

In this appendix we prove that both the total exciton population and total energy are conserved by the EXEs once the optical pulse has passed.

Using Eqs. (47)–(49), it is easy to prove the following sum rule for $Z^{\mu,\mu}_{\mu_1,\mu_2,\mu_3,\mu_4}$:

$$\sum_\mu Z^{\mu,\mu}_{\mu_1,\mu_2,\mu_3,\mu_4} = 0. \tag{A1}$$

From this sum rule and the dynamic equation (46), we can easily show that once the optical pulse has passed [i.e., $\mathcal{E}(t)=0$], then

$$\frac{d}{dt}\hat{N} = 0, \tag{A2}$$

where $\hat{N}$ is the total exciton number operator defined in Eq. (56). Thus, Eq. (A2) shows that our dynamic equations conserve total exciton number after the laser pulse has passed. We note that the factors $(1-\delta_{p,q})$ and $(1-\delta_{p,k})$ in Eqs. (48)–(50) are essential in deriving the sum rule and hence in ensuring conservation of particle number.

We can also show that the dynamic equations (40) and (46) also conserve the *energy* of the system once the laser pulse has passed. The proof of energy conservation is rather complicated in the general case (but can be done), and so we do not include it here. Instead, for demonstration purposes, we present the proof for the special case of the contact potential that we employ in Sec. IV A.

As we have explained in Sec. III C, an excitonic Hamiltonian cannot be used on its own to derive the EXEs. However, it does represent the energy of a system, which is obviously an important quantity. For our contact potential model, the Hamiltonian is given by

$$H = \sum_\mu E_\mu B^\dagger_\mu B_\mu - \frac{A}{L}\hat{N}(\hat{N}-1) - \sum_\mu \mathcal{E}(t)\cdot P_{\text{inter}}. \tag{A3}$$

For such a contact-potential interaction, there is another sum rule that must be obeyed:

$$\sum_\mu E_\mu Z^{\mu,\mu}_{\mu_1,\mu_2,\mu_3,\mu_4} = -\frac{A}{L}\sum_{k,p,q} (H^{\text{ex}}_{p,q} - H^{\text{ex}}_{k,p})(1-\delta_{p,k})$$
$$\times(1-\delta_{p,q})c^{k*}_{\mu_1}c^{p*}_{\mu_2}c^{p}_{\mu_3}c^{q}_{\mu_4}$$
$$= 0, \tag{A4}$$

where $H^{\text{ex}}_{k,p} \equiv \langle k_1|H^{\text{ex}}|k_2\rangle$ and we have used the fact that $H^{\text{ex}}_{p,q} = H^{\text{ex}}_{k,p}$ for a contact potential. In the derivation, we have also used the general relation $\sum_\mu E_\mu c^p_\mu c^{q*}_\mu = H^{\text{ex}}_{p,q}$, which is a direct result of the single-exciton eigenvalue equation,
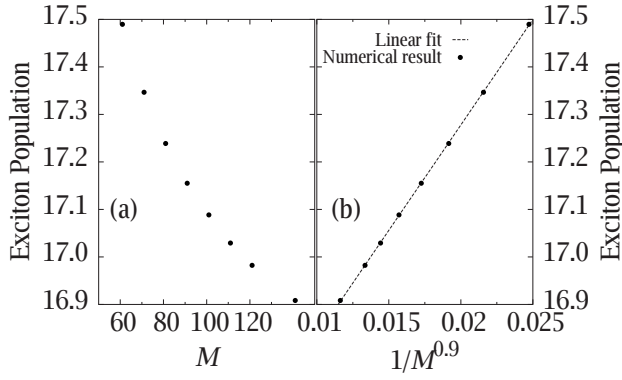
FIG. 6. (a) The total exciton population (bound and unbound) as a function of the number of exciton states, M, used in the calculation. (b) The same as (a) but plotted versus $1/M^{0.9}$. The equation of the linear fit line in (b) is given by $N = 44.38/M^{0.9} + 16.39$. The pulse intensity is the same as was used in all calculations presented in Sec. IV and all time constants were set to infinity.

$$\sum_{k_2} H^{\text{ex}}_{k_1, k_2} c^{k_2}_\mu = E_\mu c^{k_1}_\mu. \qquad (A5)$$

After the optical pulse has passed, using the sum rule of Eq. (A4), we find

$$i\hbar \frac{d}{dt} H = i\hbar \frac{d}{dt} \sum_\mu (E_\mu B^\dagger_\mu B_\mu) - \frac{A}{L} i\hbar \frac{d}{dt} [\hat{N}(\hat{N} - 1)]$$

$$= 2 \sum_{\mu_1, \mu_2, \mu_3, \mu_4} \sum_\mu E_\mu Z^{\mu,\mu}_{\mu_1, \mu_2, \mu_3, \mu_4} B^\dagger_{\mu_1} B^\dagger_{\mu_2} B_{\mu_3} B_{\mu_4}$$

$$= 0, \qquad (A6)$$

as expected. Thus, in the absence of dephasing and decay, both the total particle number and total energy are conserved by our EXEs.

We note that the sum rules of Eqs. (A1) and (A4) are only exact for an infinite exciton basis. Therefore, in numerical calculations, we need to ensure that the excitonic basis used is large enough such that energy and particle number are conserved (see the discussion in Appendix B).

APPENDIX B: THE CONVERGENCE BEHAVIOR OF EXCITON BASIS CALCULATIONS

One advantage of using a true excitonic basis is that the number of excitonic basis states required for a dynamical calculation may be very small. For example, for the system we simulated, where the pulse is resonant only with the bound excitonic state, only one excitonic state is required in the numerical calculation *if we are using a very low-intensity laser pulse*. It is important to know the convergence behavior of our results at high exciton densities where various correlation functions are potentially large. One criterion is to check if the two sum rules of Eqs. (A1) and (A4) are well satisfied for a given basis size and pulse intensity.

Since we have to use a finite number of exciton states in
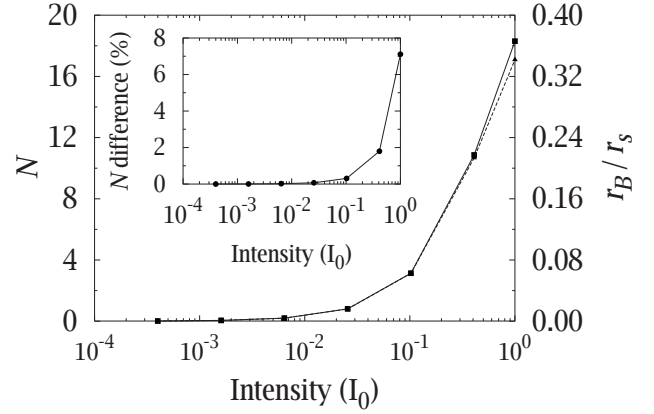

FIG. 7. The total number of excitons as a function of laser intensity, calculated using a basis of 100 excitonic states (solid squares) and a basis of 30 excitonic states (solid triangles). The y axis on the right indicates the carrier density after the pulse has passed. The inset shows the percentage difference between the carrier number calculated using bases of 30 and 100 states, respectively.

numerical calculation, the two sum rules of Eqs. (A1) and (A4) are not perfectly satisfied and this may affect our results. However, as we have shown in Sec. IV C, the conservation of total exciton number and total energy are well satisfied after the optical pulse has passed with 100 exciton states. These results indicate that the sum rules of Eqs. (A1) and (A4) are satisfied in numerical calculation with the basis size of 100 that we used.

There is, however, a third sum rule that is more difficult to satisfy with a finite basis:

$$\sum_\mu C_\mu R^\mu_{\mu_1, \mu_2, \mu_3} = 0. \qquad (B1)$$

It can be shown that a violation of this sum rule will influence total exciton number through its influence on the interband polarization. To check the convergence behavior, we plot in Fig. 6(a) the total exciton population N versus the number of exciton states used, M, when there is no decay or dephasing. We find that the total population can be fitted with a linear relation $N = 44.38/M^{0.9} + 16.39$ [see Fig. 6(b)]. From Fig. 6, we see that the total population difference between the result using $M = 100$ and $M = \infty$ is less than 4%. The small change in density is the main effect of a finite basis. For example, we find (not shown) that apart from the small scaling arising from the density differences, the calculated interband polarization is essentially unchanged when we move from 100 states to 140 states.

The $1/M^{0.9}$ dependence of the convergence for our model can be shown to be directly related to the convergence properties of the sum rule of Eq. (B1). This is a rather slow convergence. However, we have verified numerically that the convergence is strongly dependent on the system and interaction used. We have found, for example, if we use a more realistic model for the quasi-1D Coulomb interaction, it leads to an error in the sum rule of Eq. (B1) that decays *exponentially* with M. The main source of this improvement appears

to be that, in contrast to the contact potential, this potential results in several bound states. Thus, modeling the system with this potential would require a much smaller basis. We leave further discussion of this to future work.

The convergence behavior is strongly dependent on the excitation intensity, with convergence being achieved for much smaller M at lower intensities. In previous sections, we have used a high laser intensity to demonstrate clearly properties of our equations and how changes in the optical spectra can be understood in terms of excitonic population distributions. However, our excitonic approach is more efficient at low to moderate exciton densities, where the vast majority of excitons ($>85\%$) are still bound and PSF and exchange interactions are just starting to become important. At extremely low laser intensity, the excitonic approach only needs the bound exciton state for our model system. In contrast, the SBEs may still need as many states as is used with high laser intensity.

In Fig. 7, we plot the dependence of the total exciton population of the model system as a function of laser intensity. To simplify our description, we use I_0 to denote the laser pulse intensity used in Sec. IV. Starting from low intensities, we see that when we reach an intensity of about $I=0.1I_0$, the density is such that there is a significant overlap between the excitons (see scale on the right of plot). Thus, at this density, we expect that PSF effects will start to become significant. We present the total number of excitons found from calculations using a basis of 100 excitonic states (solid line) and 30 excitonic states (dashed line). As can be seen from the inset, a basis of 30 states is sufficient up to an intensity $I=0.25I_0$, where the difference between the two results is less than 2% but PSF effects are very significant ($r_B/r_s \simeq 0.22$).

[1] F. Rossi and T. Kuhn, Rev. Mod. Phys. **74**, 895 (2002).

[2] J. Shah, *Ultrafast Spectroscopy of Semiconductors and Semiconductor Nanostructures* (Springer, New York, 1996).

[3] J. Feldmann, K. Leo, J. Shah, D. A. B. Miller, J. E. Cunningham, T. Meier, G. von Plessen, A. Schulze, P. Thomas, and S. Schmitt-Rink, Phys. Rev. B **46**, 7252 (1992).

[4] V. G. Lyssenko, G. Valušis, F. Löser, T. Hasche, K. Leo, M. M. Dignam, and K. Köhler, Phys. Rev. Lett. **79**, 301 (1997).

[5] V. Klimov, S. Hunsche, and H. Kurz, Phys. Rev. B **50**, 8110 (1994).

[6] R. Takayama, N. Kwong, I. Rumyantsev, M. Kuwata-Gonokami, and R. Binder, Eur. Phys. J. B **25**, 445 (2002).

[7] H. C. Schneider, W. W. Chow, and S. W. Koch, Phys. Rev. B **70**, 235308 (2004).

[8] L. Yang, B. Rosam, K. Leo, and M. Dignam, Phys. Rev. B **72**, 115313 (2005).

[9] M. K. K. Nakaema, F. Iikawa, M. J. S. P. Brasil, E. Ribeiro, G. Medeiros-Ribeiro, J. W. Carvalho, M. Z. Maialle, and M. H. Degani, Appl. Phys. Lett. **81**, 2743 (2002).

[10] H. Haug and S. W. Koch, *Quantum Theory of Optical and Electronic Properties of Semiconductors* (World Scientific, Singapore, 1990).

[11] V. M. Axt and A. Stahl, Z. Phys. B: Condens. Matter **93**, 195 (1994).

[12] V. M. Axt and T. Kuhn, Rep. Prog. Phys. **67**, 433 (2004).

[13] M. Hawton and M. M. Dignam, Phys. Rev. Lett. **91**, 267402 (2003).

[14] M. M. Dignam and M. Hawton, Phys. Rev. B **67**, 035329 (2003).

[15] L. Yang, B. Rosam, J.-M. Lachaine, K. Leo, and M. M. Dignam, Phys. Rev. B **69**, 165310 (2004).

[16] V. M. Axt, G. Bartels, and A. Stahl, Phys. Rev. Lett. **76**, 2543 (1996).

[17] S. B. de-Leon and B. Laikhtman, Phys. Rev. B **63**, 125306 (2001).

[18] O. Betbeder-Matibet and M. Combescot, Eur. Phys. J. B **27**, 505 (2002).

[19] V. Chernyak, W. M. Zhang, and S. Mukamel, J. Chem. Phys. **109**, 9587 (1998).

[20] M. Combescot and O. Betbeder-Matibet, Europhys. Lett. **58**, 87 (2002).

[21] B. Laikhtman, Europhys. Lett. **62**, 138 (2003).

[22] M. Combescot and O. Betbeder-Matibet, Europhys. Lett. **62**, 140 (2003).

[23] T. Usui, Prog. Theor. Phys. **23**, 787 (1960).

[24] M. Hawton and D. Nelson, Phys. Rev. B **57**, 4000 (1998).

[25] J. Fricke, Ann. Phys. (N.Y.) **252**, 479 (1996).

[26] W. Schäfer, R. Lövenich, N. A. Fromer, and D. S. Chemla, Phys. Rev. Lett. **86**, 344 (2001).

[27] W. Schäfer and M. Wegener, *Semiconductor Optics and Transport Phenomena*, 1st ed. (Springer, New York, 2002).

[28] M. Combescot and O. Betbeder-Matibet, Eur. Phys. J. B **31**, 305 (2003).

[29] I. Rumyantsev, N. H. Kwong, R. Binder, E. J. Gansen, and A. L. Smirl, Phys. Rev. B **69**, 235329 (2004).

[30] P. Kner, S. Bar-Ad, M. V. Marquezini, D. S. Chemla, R. Lövenich, and W. Schäfer, Phys. Rev. B **60**, 4731 (1999).

[31] T. Meier, G. von Plessen, P. Thomas, and S. W. Koch, Phys. Rev. Lett. **73**, 902 (1994).

[32] D. S. Citrin and A. V. Maslov, Phys. Rev. B **72**, 073302 (2005).

[33] P. H. Bolivar, F. Wolter, A. Müller, H. G. Roskos, H. Kurz, and K. Köhler, Phys. Rev. Lett. **78**, 2232 (1997).

[34] A. Zhang and M. M. Dignam, Phys. Rev. B **69**, 125314 (2004).

[35] J. Hader, T. Meier, S. W. Koch, F. Rossi, and N. Linder, Phys. Rev. B **55**, 13799 (1997).